Topics in Catalysis Vol. 36, Nos. 1–4, August 2005 (© 2005)
DOI: 10.1007/s11244-005-7861-7

Looking at heterogeneous catalysis at atmospheric pressure using tunnel vision

Bas L.M. Hendriksen, Stefania C. Bobaru, and Joost W.M. Frenken*

Kamerlingh Onnes Laboratory, Leiden University, P.O. Box 9504, 2300 RA Leiden, The Netherlands

This paper addresses the "pressure gap" between traditional surface science experiments and catalysis under practical conditions. We review high-pressure, microflow experiments at elevated temperatures during the catalytic oxidation of CO. Using a specially constructed "Reactor-STM" we simultaneously determine the surface structure of a model catalyst by scanning tunneling microscopy and the reaction kinetics by online mass spectrometry. For both Pt(110) and Pd(100) we find that under O_2-rich conditions surface oxides are formed on the otherwise metallic surfaces. The presence of the oxide is correlated with a superior catalytic activity. Whereas the reaction on the metal surfaces shows traditional Langmuir–Hinshelwood kinetics, the reaction on the oxides follows the Mars-Van Krevelen oxidation–reduction mechanism, as we conclude from the reaction kinetics and the reaction-induced roughening of the surface. We emphasize that in addition to a pressure gap there can also be a temperature gap, requiring experiments to be performed not only at high pressures but also at sufficiently high temperatures.

KEY WORDS: scanning tunneling microscopy; catalysis; reaction oscillations; CO oxidation; platinum; palladium.

1. Introduction

1.1. The pressure gap

A central goal in heterogeneous catalysis research is to obtain a detailed understanding of the relation between the atomic-scale structure of a catalyst and its catalytic activity and selectivity. Surface-science studies have yielded a wealth of information about the structure of model catalyst surfaces, about atomic and molecular adsorbate and co-adsorbate geometries on these surfaces, and about the elementary atomic and molecular adsorption, diffusion, reaction and desorption processes that can take place. However, most of these studies have been carried out under the well-defined conditions of ultrahigh vacuum ($< 10^{-9}$ bar), often at room temperature or below [1]. By contrast, industrial applications of heterogeneous catalysis usually require pressures ranging from 1 to several hundred bar. This spectacular difference of typically nine orders of magnitude between laboratory and practice is commonly referred to as the "*pressure gap*". In spite of this gap, a few studies have been successful in predicting reaction rates at practically relevant pressures on the basis of information obtained at low pressures [2,3]. Of course such an extrapolation assumes that the surface is not altered by the large difference in pressure. However, *ex-situ* optical and electron microscopy observations of catalysts before and after reaction show that often massive restructuring occurs during high-pressure, high-temperature reactions [4–8] – effects that are not expected on the basis of low-pressure observations. The central question is: *What "new" phenomena occur at high pressures, and will these affect the catalytic behavior?*

* To whom correspondence should be addressed.
E-mail: frenken@physics.leidenuniv.nl

1.2. Equilibrium with the gas phase: thermodynamics

Let us first consider the effect that the presence of the gas phase, with the reactants and reaction products, may have on the equilibrium structure and composition of the catalyst surface. Obviously, at sufficiently low pressures, the surface will adopt its clean, unperturbed structure, with gas molecules occasionally adsorbing, diffusing around and desorbing again. However, at sufficiently high pressure the gas phase will play an important role in the thermodynamics of the surface. In particular, by increasing the pressure over nine orders of magnitude we raise the free energy, i.e. the chemical potential, of each gas phase molecule by $k_B T \ln(10^9)$, which amounts to as much as 0.52 eV at room temperature! This implies that the structure that would minimize the total energy of the surface plus the gas phase at low pressures may be quite different from the one that actually minimizes the *free* energy of the surface-plus-gas system at high pressures. In particular, the free energies are lowered of those structures that are formed by incorporating molecules from the high-pressure gas phase into the catalyst. How important this effect is, has been demonstrated by theoretical studies in which first-principles atomistic total energy calculations have been combined with gas-phase thermodynamics. Indeed, high-energy structures can be made thermodynamically stable at sufficiently high partial pressures of an appropriate gas [9–11].

A reaction system that has been extensively studied in this context, both experimentally and theoretically, is

CO oxidation on Ru(0001). Whereas ruthenium has a low catalytic activity for CO oxidation under UHV conditions, it shows superior activity at atmospheric pressure. By a combination of post-reaction Scanning Tunneling Microscopy (STM), Low-Energy Electron Diffraction (LEED) experiments and Density-Functional Theory (DFT) calculations it has been shown that RuO_2 is formed on the metal surface at sufficiently high O_2 pressures [12], which is held responsible for the dramatic change in catalytic performance. More recently, surface oxide structures formed at high O_2 pressures have been investigated experimentally and theoretically for surfaces of platinum [13], palladium [14–18] and rhodium [19,20]. Similar gas-pressure effects on the surface structure and composition have been demonstrated for sulfides [21] and carbides [22].

These examples of *in-situ* high-pressure experiments and "*ab-initio*" thermodynamics calculations rationalize part of the "pressure gap effect" and make it possible to understand the stability of specific surface structures in equilibrium with the gas phase of either a single component or a reactive mixture [23].

1.3. Reactions: non-equilibrium structures

Catalysis is by nature a non-equilibrium process, since the product molecules are removed and new reactant molecules are supplied continually. Each reaction event and subsequent desorption of the resulting product molecule will therefore locally bring the surface temporarily out of equilibrium. At sufficiently high turnover rates this will push the composition and structure of the catalyst surface sufficiently far away from equilibrium to affect the catalytic process noticeably and invalidate a description on the basis of equilibrium thermodynamics. This forces us to consider the surface structure during actual reaction.

Kinetic, i.e. non-equilibrium effects are illustrated beautifully in (spatio)-temporal oscillations in the reaction rate [24]. For example during CO oxidation at low pressures the Pt(110) surface can switch between a reconstructed 1×2 surface and a 1×1 structure, depending on the coverages of the two reactant species O and CO. Because the 1×1 surface exhibits a higher reaction rate, the CO_2 production switches too. The coupling between the structure and the rates of the individual processes leads to self-sustained oscillations in time (and in space) of the surface structure, the adsorbate coverages, and the reaction rate. Closely related to this reaction-induced $1\times2\leftrightarrow1\times1$ modulation of the surface structure is spatial pattern formation by microfacetting, induced by the CO oxidation reaction and leading to an increase in catalytic activity [25,26]. These structures are only 'stable' during the reaction and can therefore be studied only *in situ*.

Also at atmospheric pressure CO oxidation on Pt-group metals exhibits self-sustained oscillations in the reaction rate. These high-pressure oscillations have been attributed to the periodic formation and removal of a non-active oxide, leading to a periodic decrease and increase in the reaction rate [27–29], a scenario that differs completely from that of the low-pressure oscillations. Oscillating reactions clearly manifest the relation between (changes in) the surface structure and composition of a catalyst and (changes in) the catalytic activity. They further demonstrate the importance of investigating the surface structures during the reaction, even under nominally steady-state conditions.

1.4. In-situ *techniques: high pressure-STM*

Most surface-sensitive analysis techniques are based on electron, ion or molecular beams, which inherently restricts their maximum operating pressure. By using differential pumping stages, one can extend the pressure ranges of these techniques, such as X-Ray Photoelectron Spectroscopy (XPS), Low-Energy Ion Scattering (LEIS), and Transmission Electron Microscopy, in favorable cases even up to several millibar [30–32]. A variety of surface-sensitive optical spectroscopy and microscopy techniques has been applied to catalytic surfaces at atmospheric pressures [33–37]. X-Ray Absorption Spectroscopy and Surface X-Ray Diffraction (SXRD) have been used successfully to resolve the electronic and atomic structures of catalytic surfaces at elevated pressures in single-component gasses or during reaction [38,39].

The STM is one of the few instruments that can resolve atomic-scale structural information of a surface both in vacuum, at atmospheric pressures and beyond. It has been shown by McIntyre that STM observations are possible at atmospheric pressures of reactive gasses, simply by backfilling a UHV chamber [40]. Several groups have followed this approach [41–44]. High-Pressure STM (HP-STM) has made it possible to image adsorbate structures at high pressures, e.g. of CO on Pt(111) [45,46], and of CO and NO on Rh(111) [47–49]. Also, gas-phase-induced restructuring of metal surfaces has been observed by HP-STM, for example of Pt(110)-1×2 in CO [50], H_2 and O_2 [51], and of Cu(110)-1×1 in H_2 [52]. Supported gold nanoparticles in TiO_2 have been studied in mixtures of CO and O_2 over a wide pressure range [53].

Although the examples mentioned here have already explored the "other side" of the pressure gap, the emphasis has been on *single-component* gasses and *room temperature*. Of course, the next stage is to observe structures and processes that occur during catalytic reactions in high-pressure *reactant mixtures at elevated temperatures*. In order to enable STM-observations under such conditions, we have followed an alternative approach. Instead of pressurizing a complete, large-volume vacuum chamber, which behaves as a so-called 'batch reactor', we have integrated a miniature

STM with a small-volume micro-flow reactor [54,55]. In the following, we briefly describe the resulting Reactor-STM setup and give an overview of the *in-situ* observations obtained with this instrument during the catalytic oxidation of CO on platinum and palladium surfaces at atmospheric pressures and elevated temperatures.

2. Experimental

2.1. Reactor-STM

Integrating a HP-STM with a micro-flow reactor introduces the possibility to directly observe the correlation between (changes in) the surface structure and (possible variations in) the catalytic performance. Ideally the minimum time needed to measure the reaction product concentration is comparable to the time required to record an STM image (or a single scan line), which is a few seconds up to a minute. This puts a severe restriction on the geometry of the instrument, since the area of a typical, single-crystal model catalyst surface is small, typically 1 cm^2, corresponding to 'only' $\sim 10^{15}$ surface atoms as potential reaction *sites*. The turnover rate of the chemical reaction probably will be in the range of 10^{-4}–10^{2} product molecules/site/s [2]. If we assume a minimum turnover rate of 10^{-2} at $T = 425$ K, combined with a detection limit of a mass spectrometer of 1 ppm, this means that the maximum gas flow containing 1 ppm reaction product is 10^{15} sites $\times 10^{-2}$ molecules/site/s $\times$ 10^{6} = 10^{19} molecules/s, which according to V = NRT/P corresponds to a volume flow of $\sim$0.5 ml/s at a pressure of 1 bar at that temperature. In other words, if we require a time resolution of 1 s, i.e. a refresh rate of 1 reactor-volume/s, at a product concentration of 1 ppm, we need the reactor volume to be at most 0.5 ml, which is much smaller than the size of a typical STM head. In order to still meet the small-volume requirement, we have combined an STM with a micro-flow reactor in such a way that only the STM tip is mounted inside the reactor, which therefore can be reduced to 0.5 ml [54,55]. The other parts of the STM, i.e. the scanner, etc, are separated from this reactor volume by a tiny Viton® O-ring seal.

A schematic of the reactor-STM combination is shown in figure 1. The STM-tip is mounted in a small capillary that is situated in an aluminum tube, which is closed at the bottom and is glued to the piezo tube scanner. A ridge on this aluminum tube is used to clamp the O-ring against the bottom wall of the reactor. The O-ring provides a gas-tight seal, yet it is flexible enough to allow the full range of the scanning motion of 3 μm. The top side of the reactor is formed by the surface of the model catalyst sample. A gas-tight seal between the sample and the rest of the reactor is established by a Kalrez® seal, against which the surface is pressed. All reactor walls have been made inert by gold plating, in order to avoid chemical reactions on other surfaces than that of the sample. There are several additional advantages in the geometry of our Reactor-STM. For example, pressing the sample surface against the Kalrez® seal ensures that only the surface orientation of interest can contribute to the catalytic reaction. Since the piezo element and other components of the STM are not in contact with the hot, reactive gasses, there is no risk of reaction-induced damage to the microscope. Similarly, since the piezo element is not in contact with the hot gas, the microscope can operate at a substantial temperature difference between the hot sample and gas and a relatively cool piezo element, thus avoiding depolarization

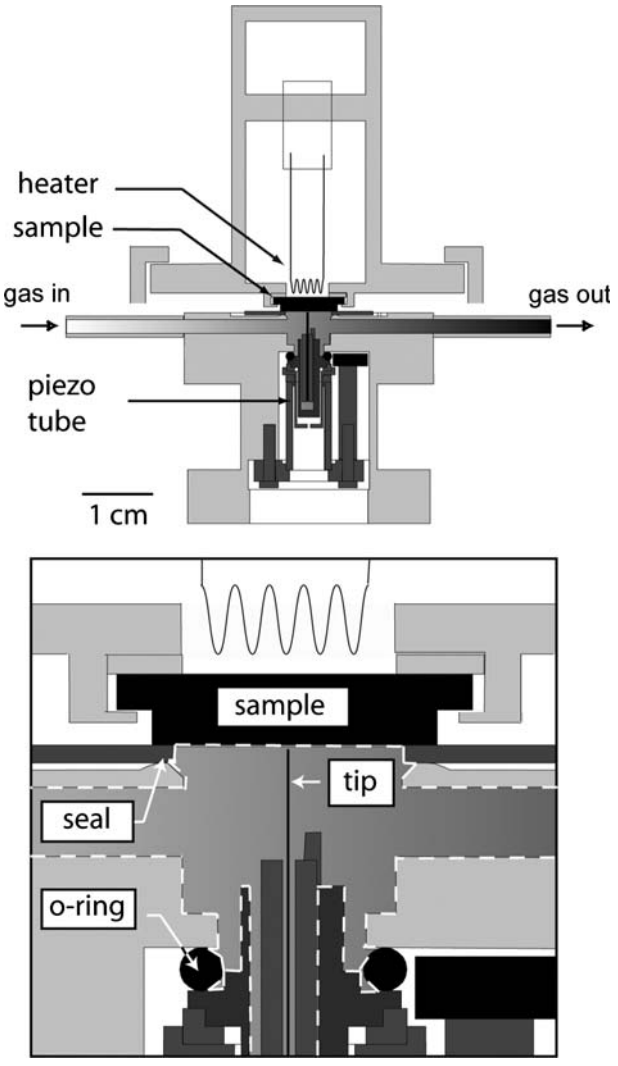

Figure 1. Schematic cross section of the 'Reactor-STM'. The instrument can image a surface, while it is active as a catalyst, under gas flow conditions at pressures up to 5 bar and temperatures up to 500 K. Apart from the surface of the sample, only the tip of the STM is in contact with the flowing, hot, high-pressure gas mixture. The blow-up shows how the scanning motion, generated by the external piezo element, is transferred to the STM tip inside the reactor cell via a flexible Viton® o-ring. The upper side of the reactor is closed by the sample surface that is pressed against a Kalrez seal. The volume of the cell, which is indicated by the dashed white line, is as small as 0.5 ml (after [55]).

of the piezo element when it would otherwise pass its Curie temperature. Finally, since the geometry of the tiny reactor is relatively simple, there is no strong degradation of the time resolution of the gas composition measurement due to stagnating parts in the flow distribution in the reactor.

The reactor-STM combination is mounted on a 8″ vacuum flange as part of an ultrahigh vacuum (UHV) system. In the UHV system, we can prepare surfaces by means of ion bombardment and high-temperature annealing. The UHV chamber further contains a combined LEED and Auger Electron Spectroscopy (AES) system, which can be used for surface analysis in UHV before and after a high-pressure experiment. The UHV setup also contains the Quadrupole Mass Spectrometer (QMS), which we use to analyze the gas flow from the reactor. The sample can be transferred to the reactor without breaking the vacuum. In the reactor the sample can be heated safely to a maximum temperature of about 500 K by a filament located at the rear side of the sample (i.e. at the UHV side), which is integrated in the sample holder. After each substantial temperature change, it takes approximately 2 h for the thermal drift to become low enough for meaningful STM observations. The pressure can be varied from vacuum to 1 bar at high temperature without additional thermal drift.

We use a dedicated gas manifold to operate the reactor in flow mode with gas flows up to 10 ml_n/min, i.e. typically 1/3rd reactor-volume/s, at pressures of 0.1–5.0 bar. The gas manifold allows us to control independently the composition of the gas, the pressure in the reactor, and the flow rate. The hard, mechanical connection that the gas tubes establish to the reactor, and therefore also to the STM, prevents us from using internal vibration isolation between the UHV chamber and the STM, e.g. by means of spring suspension. Obviously, this compromises the resolution of the STM. Nevertheless, the compact design of the STM makes the mechanical path between tip and sample rather short and stiff, so that atomic resolution on graphite (HOPG) and step resolution on metal surfaces are still achieved routinely.

3. Results and discussion

3.1. Pt(110) during CO oxidation

We start this review of results obtained with our Reactor-STM with the oxidation of CO on Pt(110). This surface has been studied at high gas pressures with STM by at least three research groups [13, 50, 51]. Under UHV conditions, it exhibits the so-called 1×2 missing-row reconstruction, in which every second atom row along the close-packed $[\bar{1}10]$ direction is absent. The surface can be regarded as a regular array of tiny (111) facets. At low pressures, adsorption of CO on this surface lifts the reconstruction and stabilizes a 1×1 bulklike termination of the crystal. CO oxidation on Pt(110) at low pressures has been studied extensively as it exhibits (spatio) temporal oscillations, which originate from adsorbate-induced restructuring [56].

In their pioneering work McIntyre *et al.* have shown that Pt(110) restructures in single-component gasses of hydrogen, oxygen and carbon monoxide also at atmospheric pressures and at 425 K. They found that in 1 bar of CO the surface had flat (110) terraces separated by steps of multiple-layer height; in 1 bar of O_2 the surface had formed (111) facets and in 1.6 bar H_2 the surface appeared to be characterized by various sizes of nested missing-row type structures. Later, Thostrup *et al.* found that CO adsorption lifted the missing-row structure and restored the (1×1) bulk terminated structure, but they did not observe multi-atomic step heights. The lifting of the missing-row structure was accompanied by the formation of (monatomic) steps, of which the density increased until the CO-adsorbate coverage reached 70%. For higher CO coverages the step density decreased again. The main effect of the high pressure was to establish high adsorbate coverages, similar to low-pressure, low-temperature experiments. Thostrup *et al.* concluded that over a pressure range of 12 orders of magnitude in pressure the surface responded very similarly to exposure to CO.

Also with our Reactor-STM we have observed that Pt(110) in pure CO at 1 bar and 425 K restructures from the 1×2 missing-row pattern to the 1×1 bulklike structure [55]. Figure 2 shows a series of snapshots from an STM movie, taken during this process (movies related to this paper can be viewed on the group webpage [57]). Although the transition from 1×2 to 1×1 is complete already in the first panel of figure 2, immediately after introduction of the CO gas, the surface is still far from equilibrated. This is caused by the fact that the local $1\times2 \rightarrow 1\times1$ rearrangement has left the top layer only half occupied, which necessarily introduces a high density of steps. The second and later panels illustrate the coarsening of the step configuration that takes place afterwards, driven by the energy lowering that accompanies the reduction in step density. The final result is a smooth, CO-covered Pt(110)-1×1 surface, which serves as a well-defined starting configuration for the CO oxidation experiment, illustrated in figure 3a.

In the CO oxidation experiment we changed the gas flow from pure CO to an O_2-rich mixture of CO + O_2 and back again to pure CO [13]. The middel panel of figure 3 displays a selection of STM images from an STM movie that was recorded during such a $CO \rightarrow CO + O_2 \rightarrow CO$ sequence [57]. The lower panel shows the signals from the quadrupole mass spectrometer (QMS) for the reactants, CO (28 atomic mass units) and O_2 (32 amu), and the reaction product, CO_2 (44 amu), that were recorded simultaneously with the STM movie. At $t = 140$ s we closed the valve of the CO gas line and opened the valve of the O_2 line, which

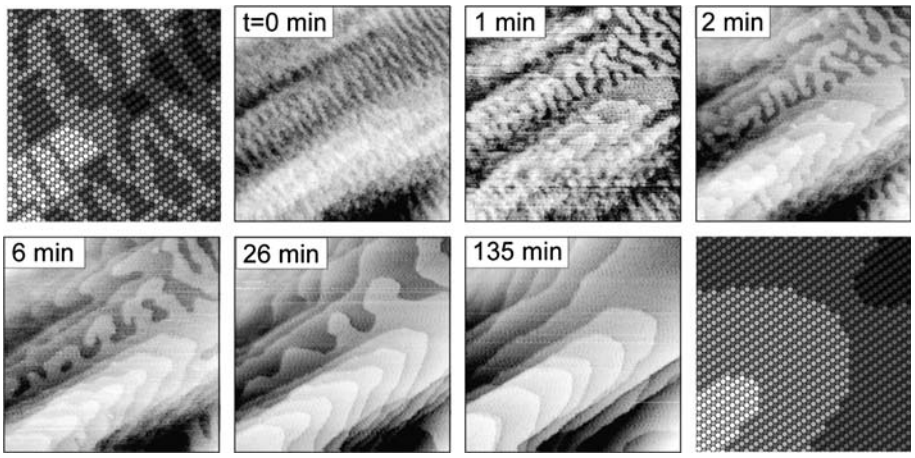

Figure 2. Series of STM snapshots (140 nm×140 nm) taken on Pt(110), starting immediately after introduction of 1.25 bar CO in the Reactor-STM at 425 K. The 'tiger skin' pattern in the first panel shows that the 1×2 to 1×1 transition has divided the surface in two levels, each 50%, and a high density of steps. Subsequent images show the progressive reduction of the step density by coarsening of the step pattern. The elapsed time in min. is indicated in each panel. The two ball models indicate the atomic-scale geometries characteristic for the starting and end situations (after [55]).

resulted in a steep increase in the O_2 signal at $t = 502$ s and a corresponding decrease of the CO signal. The time delay and the long presence of a small, residual fraction of the initial partial pressure of CO reflect the time constant of our gas handling system. With CO and O_2 both present in the reactor, the surface immediately started to produce a modest amount of CO_2 (R_{metal}), as can be read off from the CO_2 signal in the bottom panel of figure 3. Nevertheless, the STM image in figure 3b shows that the surface structure had not changed noticeably. The CO_2 signal saturated at a level of 0.5 mbar and stayed constant, even though the partial pressure of CO decreased. After $t = 1800$ s several instabilities were observed in the CO_2 production, which heralded an abrupt increase in CO_2 production rate by a factor 3 at $t = 2109$ s. This sudden step in reaction rate occurred during the acquisition of image 3c. The image was scanned from bottom to top in 65 s. The lower ¼ of the image, just before the step in the rate, still showed the metallic Pt(110)-1×1 surface. During the upper 3/4 of the image the surface already had the increased reactivity. The sudden change in thermal drift in the z-direction of the image, caused by the small temperature increase accompanying the step up in the exothermic reaction, made it possible to accurately synchronize the STM measurement with the QMS signals to within a single scan line, i.e. to within 1 s. The upper 3/4 of image 3c showed a modest, uniform change of the surface corrugation with respect to the lower 1/4 of the image, but no dramatic, e.g. large-scale restructuring was observed. As will be discussed further below, we conclude that the upper 3/4 of the image corresponded to a thin, commensurate platinum oxide film. The stepwise increase of the reaction rate was caused by the formation of this surface oxide that clearly had a higher catalytic activity. After the switch, the CO_2 production rate (R_{oxide}), now catalyzed by the platinum oxide surface, decreased proportional to the CO partial pressure. Since the formation of the oxide did not introduce adatom islands, vacancy islands, or systematic shifts in step positions, we conclude that the areal density of Pt atoms in the oxide was equal to that of an integer number of Pt(110) monolayers.

The initially flat oxide surface gradually became rough during the high-reactivity phase ($2109 \text{ s} < t < 2913$ s), as can be seen from images 3c and d and from the top panel of figure 3, in which we have quantified the accumulated (root-mean-square) roughness, as measured on single terraces. Within the statistics of the measurement, the rms roughness increase was proportional to the total amount of CO_2 produced. This strongly suggests that the roughness was a reaction 'product'. The roughness consisted of pits and protrusions with apparent diameters of 40–70 Å. The heights were in the range of 2–4 Å, but they did not correspond to single or multiple steps on Pt(110). The roughening of the oxide surface was observed only in CO + O_2 mixtures, during the CO oxidation reaction, and not in pure O_2.

Based on the evidence given above and further evidence, not shown here [13,55], we propose that the CO oxidation reaction on the surface oxide followed the Mars-Van Krevelen oxidation–reduction mechanism [12,58–60]. When applied to CO oxidation, this mechanism works as follows (see figure 4). CO molecules from the gas phase react with oxygen atoms in the oxide lattice to form the CO_2. Each oxygen vacancy that this process leaves behind in the oxide, is refilled quickly with oxygen from the gas phase or from other parts of the oxide. In this way, the catalytic reaction proceeds via a continuous and local reduction and (re-)oxidation of the oxide surface. This process can lead to roughness if it

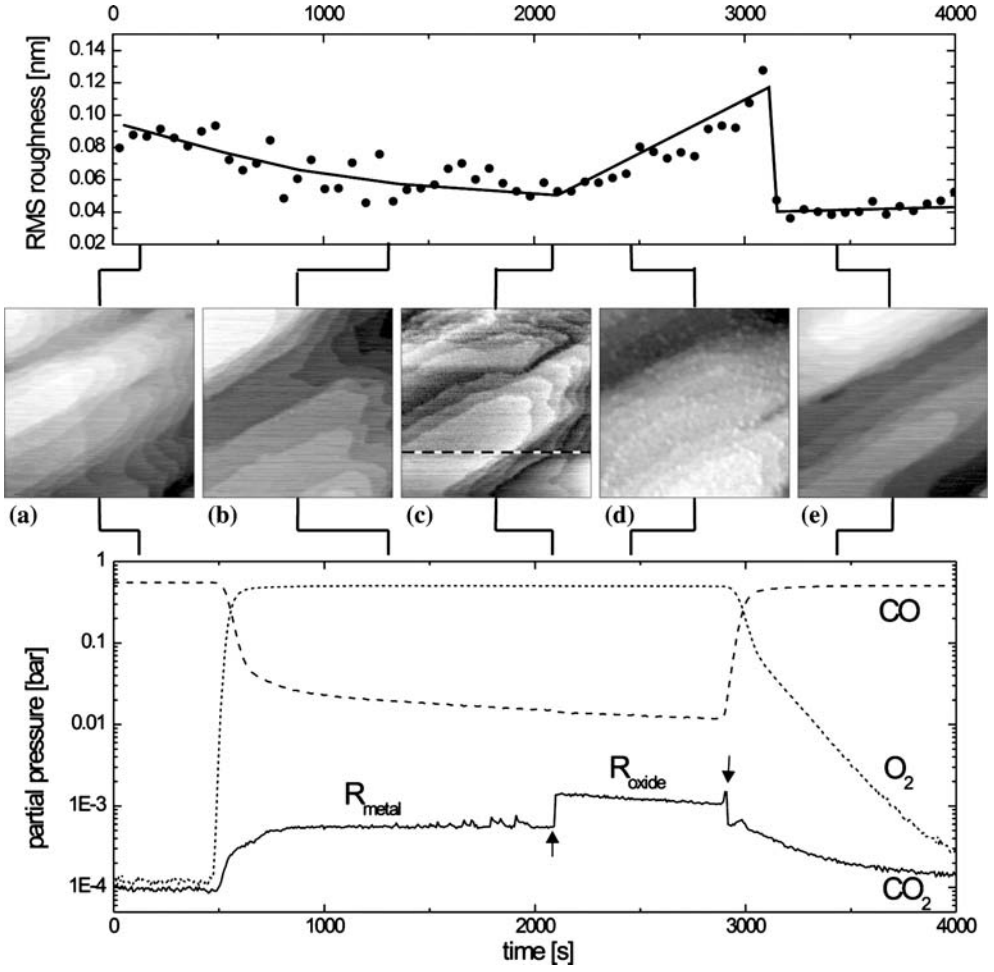

Figure 3. STM images and mass spectrometer signals measured simultaneously during CO oxidation on Pt(110) at a temperature of 425 K in a 3.0 ml/min flow of a CO and O_2 gas mixture at a total pressure of 0.5 bar. (Top panel) The root mean square roughness evolution on a terrace. The solid line is a guide to the eye. (Middle panel) A selection of STM images (210 nm × 210 nm, $I_t = 0.2$ nA, $V_t = 80$ mV) from an STM movie [57]. Images (a), (b), the lower part of (c), and image (e) show the metallic, mainly CO-covered Pt(110) surface. The upper part of image (c) and image (d) represent the oxide surface which gradually roughened. (Bottom panel) Partial pressures of the reactant gasses CO and O_2 and the reaction product CO_2. R_{metal} denotes the reaction rate on the metallic surface and R_{oxide} is the rate on the oxide surface. The arrows indicate where the surface switched from metal to oxide (pointing up) and back (pointing down) (after [13]).

occasionally leaves one of the Pt atoms so strongly under-coordinated that it diffuses out of the oxide. Of course, the diffusing Pt atom will be oxidized eventually, but now on top of the oxide. Since the rate at which the roughness built up was much lower (roughly factor 500) than the CO oxidation rate, we can consider the roughness to be a minor byproduct of the reaction. The presence of the roughness itself did not affect the measured reaction rate. The observed reaction-induced roughness formation is reminiscent of catalytic etching [5] and oxidation–reduction induced roughening in electrochemical experiments on Pt electrodes [61].

At $t = 2913$ s we closed the O_2 valve of the gas system and simultaneously opened the CO valve, to return to a pure CO flow. The CO_2 signal initially increased, proportional to the CO pressure, resulting in a small, upward spike. After this it stepped down to the CO_2 pressure level corresponding to the reaction rate on the metallic surface. The CO_2 signal then decreased hand in hand with the reducing partial pressure of O_2. Figure 3e shows that after the switch to the pure CO flow, also the STM images corresponded to the metallic surface, with well-defined terraces and steps with the familiar step height of Pt(110). Immediately after the switch, i.e. before image 3e, the metal surface exhibited residual roughness in the form of Pt adatom islands and vacancy islands. This shows that indeed Pt atoms had been redistributed during the CO oxidation, in accordance with the Mars-Van Krevelen based roughening scenario described above. The islands rapidly decayed with time to finally restore flat 1 × 1 terraces, similar to the starting situation (figure 3e).

A variety of platinum (surface) oxides on Pt(110) have been reported [62–64], based on *ex-situ* experiments and DFT calculations. Separate DFT calculations show reaction paths on these oxides with extremely low

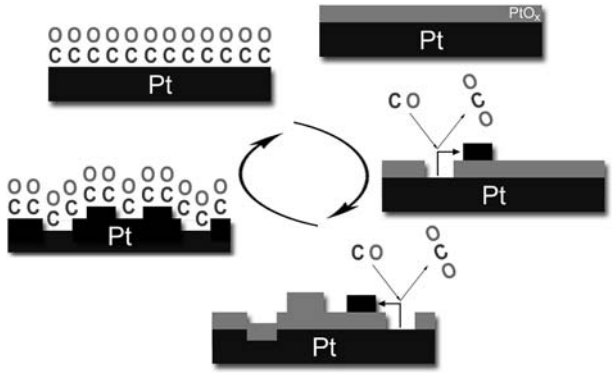

Figure 4. Schematic of reaction mechanisms for CO oxidation on Pt(110). At low partial pressure of oxygen the Pt(110) surface is smooth and almost fully covered by a dense, CO overlayer (upper left). CO reaction proceeds via the Langmuir–Hinshelwood mechanism with dissociatively adsorbed oxygen. At sufficiently high oxygen pressure a thin surface oxide is formed (upper right). Reaction now takes place between CO molecules and oxygen atoms that are removed from this oxide (centre right). Occasionally, an undercoordinated Pt atom diffuses out of the reduced region, to be oxidized on top of the oxide, making the oxide surface increasingly rough (bottom). When exposed to a high CO pressure, the rough oxide is removed by the reaction and a rough metallic surface remains (centre left), which quickly becomes smooth to restore the initial situation (upper left).

activation barriers [65,66] (B. Hammer, Private communication).

In order to obtain further verification for the presence of a surface oxide and to resolve its atomic structure, we have repeated our high-pressure experiments with Surface X-Ray Diffraction (SXRD) at the European Synchrotron Radiation Facility (ESRF) in Grenoble. These experiments have been performed under very similar conditions, during CO oxidation at high pressures and high temperatures on Pt(110). Again the structure measurements, in this case diffraction, were combined with QMS measurements of the reaction kinetics, but now in batch-reactor mode. The SXRD data are in full agreement with the STM observations and show that a special, CO-stabilized platinum surface oxide is formed. They further allow us to infer that this oxide is precisely 1 monolayer thick, that it is indeed commensurate with the Pt(110)-1×1 surface, and that it has a 1×2 periodicity. Further details about this structure will be reported in a future publication [67].

One may wonder to what extent these results are specific for the present choice of surface orientation of the model catalyst. In order to investigate this point we have performed similar STM and SXRD experiments on the (111) surface of platinum [68,69]. Our results show behavior that is quite similar to that on Pt(110). Again, depending on the partial pressures of O_2 and CO, the surface can be made to switch between a metallic state with a modest reactivity and an oxidic state with a high reactivity. The oxide gradually roughens during the reaction, while the metal tends to become smooth. This similarity between the open and close-packed surfaces of platinum at atmospheric pressure stands in contrast with the striking orientation dependence that is known at low pressures.

3.2. Pd(100) during CO oxidation

The kinetics of CO oxidation on palladium catalysts is very similar to that on platinum catalysts, as has been found already more than two decades ago by experiments with model catalysts in the form of polycrystalline palladium or platinum wires [27,28]. This makes it natural to expect a similar mechanism on palladium, again involving a surface oxide and the Mars-Van Krevelen oxidation–reduction mechanism. The stability and importance of oxides have been established already much more for palladium than for platinum and there has already been a long debate about which phase would be more catalytically active for the oxidation of hydrocarbons (i.e. methane) [70]. From extensive investigations, involving LEED [71], STM [72], Core-Level Photoelectron Spectroscopy combined with DFT [73], and SXRD [17,18], it is known that Pd(100) forms a thin $\sqrt{5}\times\sqrt{5}$ R27° oxide structure at low oxygen pressure, followed by the formation of thicker layers of bulk PdO at higher O_2 pressures and higher temperatures. The bulk PdO has its (001) plane parallel to the Pd(100) substrate and it has the same azimuthal alignment as the $\sqrt{5}\times\sqrt{5}$ R27° structure. The $\sqrt{5}\times\sqrt{5}$ R27° structure has a mismatch in Pd atom density of 20% with the Pd(100) surface. Therefore, the formation of this thin oxide leads to the expulsion of 1/5th of a monolayer of excessive Pd atoms, which results in an oxide film with 20% in higher-level islands. In contrast to the case of the thin, commensurate surface oxide on Pt(110), the mismatch of the thin oxide on Pd(100) makes that not only the Mars-Van Krevelen mechanism but already the oxidation process itself introduces surface roughness.

Figure 5a shows an STM image of the metallic Pd(100) surface in a flow of CO + O_2. As in figure 3, the second panel of figure 5 contains the mass spectrometry signals of CO, O_2 and CO_2. The metallic palladium surface consisted of flat terraces, separated by mono- and multi-atomic steps that ran preferentially along the [011] direction. The partial pressure of CO was decreasing slowly and the signal of the reaction product CO_2 followed this decrease until t = 578 s, at which point we observed a step up in the CO_2 production rate by a factor 1.5. This upward step occurred during the recording of the scan line indicated by the dashed line in figure 5b. The part of the image that was recorded after the switch (the upper 1/4th of the image) shows both the original steps and a high density of newly formed, small islands. Similar to the case of Pt(110) we attribute the stepwise increase in the reaction rate to the Mars-Van Krevelen mechanism, which sets in as a result of the oxidation of the surface. The sudden appearance of

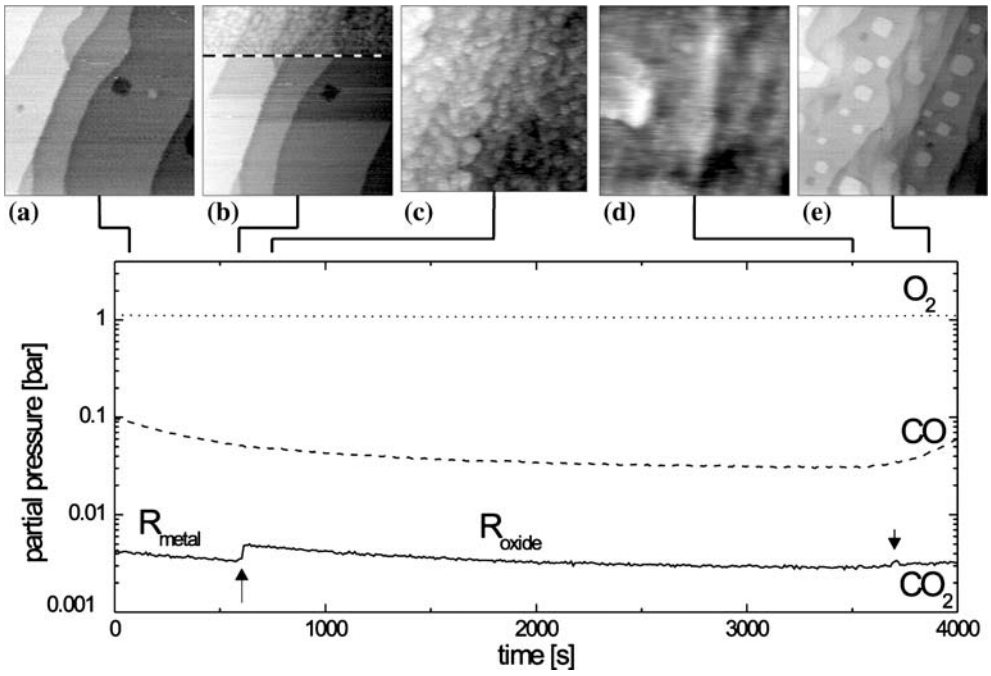

Figure 5. STM images and mass spectrometer signals measured simultaneously during CO oxidation on Pd(100) at a temperature of 408 K in a 5.0 ml/min flow of a CO and O_2 gas mixture at a total pressure of 1.25 bar. (Top panel) A selection of STM images (140 nm×140 nm, I_t = 0.2 nA, V_t = 112 mV) from an STM movie [57]. Image (a), the lower part of (b), and image (e) show the metallic, mainly O-covered Pd(100) surface. The upper part of image (b), and images (c) and (d), represent the oxide surface. (Bottom panel) Partial pressures of the reactant gasses CO and O_2 and the reaction product CO_2. R_{metal} indicates the reaction rate on the metal surface and R_{oxide} is the rate on the oxide surface. The arrow pointing up marks the switch from the metal to the oxide, the arrow pointing down marks the switch from the oxide to the metal (after [15]).

islands, covering approximately 20% of the surface, reflects the Pd atom density mismatch expected for the $\sqrt{5}\times\sqrt{5}$ R27° surface oxide, referred to above. In the oxide phase, the CO_2 production decreased proportional to the CO pressure and additional roughness gradually built up on the oxide surface. The mismatch-induced roughness with which the oxide was formed complicated a quantitative analysis of the reaction-induced roughness formation, of the type performed for Pt(110). An additional complication is that under similar conditions the oxidation of Pd(100) has been found not to stop. As described above, a thick, bulklike PdO(100) film may form. Again, there is a difference in areal density with the Pd(100) substrate, which implies that such bulk oxidation would inherently create roughness [18]. At t = 3680 s we increased the CO pressure again. As a result, the surface switched back to its metallic form, as can be seen in figure 5e, which shows steps and islands with multiples of the step height of 1.95 Å, characteristic for metallic Pd(100). The islands decayed with time to restore the flat Pd(100) surface. The CO_2 signal had a tiny maximum (indicated by the arrow) before the transition to the metallic phase.

The difference between the reaction rates on the oxide and the metal may seem rather small. However, it should be emphasized that these observations have all been performed at a temperature that is, from a catalysis point of view, still relatively low. Experiments performed at higher temperatures in a separate setup, not involving an STM, showed much more dramatic differences in reaction rate.

3.3. Reaction kinetics, bistability and oscillations

Figures 6a and b provide a more systematic view of the dependence of the reaction rate on the partial pressure of CO, for Pt(110) and Pd(100), respectively. In complete accordance with the more anecdotal description, given in the previous sections, the data in figure 6 separate into two distinct branches. For both metals, all STM images taken simultaneously with measurements on the lower branch showed the surface in its metallic form, while the higher branch corresponded exclusively to the presence of the surface oxide. What figure 6 clearly shows is that there is not only a quantitative difference between the branches, the oxide being more reactive than the metal, but that there is also a qualitative difference, the type of relation between CO pressure en CO_2 reaction rate being different as well. This implies that the reaction kinetics are not the same, suggesting that the reaction mechanisms on the metal and the oxide are different.

Let us first consider the upper branch (R_{oxide}), for which the reaction rate on the oxide depends in a

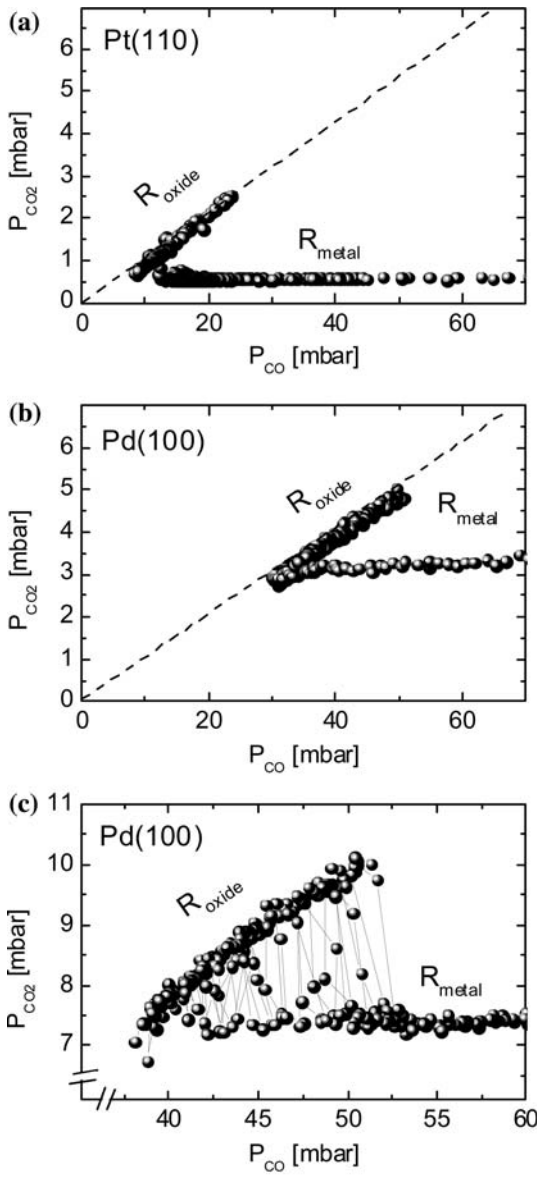

Figure 6. The CO_2 production (P_{CO_2}) as a function of the CO pressure (P_{CO}) at a nearly fixed oxygen pressure (P_{O_2}) for (a) Pt(110) at P_{O_2} = 0.5 bar and T = 425 K, and (b) and (c) Pd(100) at P_{O_2} = 1.25 bar and T = 408 K. For both surfaces the data separate into two reaction rate branches, one that corresponds to the metal (R_{metal}) and one that corresponds to the oxide (R_{oxide}). The reaction rate branches overlap over a CO pressure range of roughly 20 mbar. This makes the system bistable for fixed P_{CO} and P_{O_2}, which can lead to spontaneous switching between the metal and oxide branches as shown in (c), causing the self-sustained reaction rate oscillations (after [75]).

surprisingly simple manner on the partial pressures P_{O_2} and P_{CO} of O_2 and CO. On both Pt(110) and Pd(100), the CO_2 production rate was found to be independent of P_{O_2} and proportional to P_{CO}. In the light of the proposed Mars-Van Krevelen mechanism, this should come as no surprise, since in this oxidation–reduction mechanism the oxygen is not provided directly by the gas phase or via a surface-adsorbed species of which the surface coverage would depend on P_{O_2}. Instead, oxygen is supplied by the oxide. As long as the oxide is thermodynamically stable, which is the case for a range of P_{O_2} and P_{CO} values at each temperature, the reaction rate should not vary with P_{O_2}. Since the formation of a CO_2 molecule requires a single CO molecule, the kinetics should be first-order in P_{CO}, which is reflected in the direct proportionality between P_{CO_2} and P_{CO}.

We now turn to the lower branch (R_{metal}). On Pt(110), the reaction rate on the metal was virtually independent of P_{CO}, while there was a weak dependence for Pd(100). In fact, for higher partial pressures of CO, beyond the scale of figure 6b, the reaction rate on Pd(100) went through a maximum, after which it reduced again. On both metals, the dependence of P_{CO_2} on P_{CO} could be described by the familiar Langmuir–Hinshelwood kinetics, in which O atoms and CO molecules compete for adsorption sites on the surface and the rate of CO_2 formation is proportional to the product $\theta_O\theta_{CO}$ of the surface coverages of the two species. The difference between the two metals is that over the range of conditions on the lower branch in figures 6a and b, the Pt(110) surface is covered by a dense CO adsorbate layer with a very low density of co-adsorbed O-atoms, i.e. $\theta_{CO} \gg \theta_O$, while the Pd(100) surface is covered by a mixture of O and CO adsorbates with $\theta_O > \theta_{CO}$.

A remarkable aspect of figures 6a and b is that in both cases the two reaction branches overlapped over a significant range in CO pressure. In other words, the reaction system appeared to be bistable within this CO pressure window. In figure 6c we see that for Pd(100) this bistability sometimes led to oscillations in the reaction rate, which was found to switch spontaneously back and forth between the low-reactivity metallic branch and the high(er)-reactivity surface oxide branch [74].

The existence of two distinct branches in reaction rate, bistability and reaction oscillations had been observed previously, e.g. for polycrystalline wires of Pt, Pd and Ir, albeit with an incorrect interpretation of the surface structure and reaction mechanism underlying the high-reactivity branch [27,28]. We can use our combination of STM images and kinetic data to re-interpret the existing literature on flow experiments for a variety of model catalysts under a variety of conditions. For example, we can take the observations of Turner *et al.* [27,28] to conclude that also at much higher temperatures and much higher P_{CO}/P_{O_2} ratios, i.e. possibly also under the conditions at which three-way car catalysts operate, the surface oxides should form the active phase on platinum and palladium surfaces. We further conclude that the well-known, self-sustained rate oscillations observed during CO oxidation at atmospheric pressure on e.g. Pd surfaces are caused by a spontaneous cycle of collective oxidation and reduction of the metal surface, with the oxide forming the more active phase. These conclusions are in stark contrast with the established models for bistability

at atmospheric pressures [27,28] and for oscillations on Pd at both low and high pressures [75,76].

3.4. A case for high temperatures

We close this review of STM results obtained at high pressures by a word of caution, in order to stress the importance of also going to elevated temperatures. Figure 7a shows an STM image obtained on the Pt(111) surface in a pure CO flow at 1.25 bar and room temperature. The regular array of bumps in the image has a period of 1.2 nm, which is much larger than the interatomic distance on the platinum surface or the expected distance between adsorbed CO molecules. Superimposed on the bumps, a second structure with a much smaller period is vaguely visible in the image. Higher-resolution STM and LEED observations have been made before for this configuration of CO on Pt(111) [45,46,77] and it has been found to correspond to the Moiré pattern between a $\sqrt{19}\times\sqrt{19}$ R 23.4°, close-packed CO overlayer and the Pt(111) substrate. Figure 7b shows a similar image with the same Moiré pattern, but in this case the image was recorded under nominally pure O_2 conditions at room temperature. Although the O_2 gas was not contaminated by more than 0.1% CO (estimated upper limit), this contaminant completely dominated the adsorption at room temperature, thereby poisoning the surface for interaction with O_2. Similar CO poisoning has been observed by high-pressure STM for ethylene hydrogenation [78]. However, the CO structure of figure 7b was "prepared" by first deliberately oxidizing the Pt(111) surface in an O_2-rich flow at 425 K, after which the surface was cooled to room temperature in almost pure O_2 for the purpose of studying the oxide structure at room temperature [68]. The fact that we obtained a CO-covered metal surface instead illustrates that the structure that is active *during* a reaction may differ substantially from structures studied *after* the reaction, in this case after cooling down to room temperature. The oxide on Pt(111) was only stable at elevated temperatures and during the cooling down, the low, but non-zero CO concentration in the O_2 gas flow was sufficient to reduce the surface to the metallic state and populate it with a densely-packed CO overlayer.

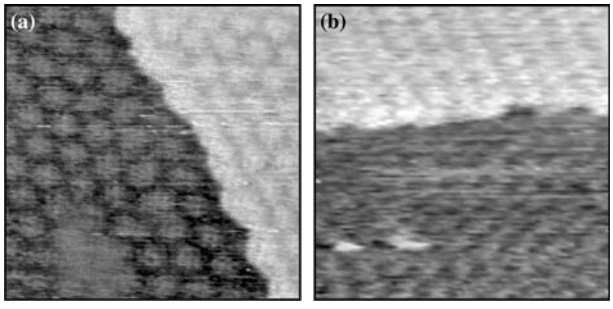

Figure 7. STM images (10.6×10.6 nm) of a Moiré pattern with a periodicity of 1.2 nm on Pt(111) caused by a $\sqrt{19}\times\sqrt{19}$ R23.4° CO overlayer [46] (a) imaged in pure CO at P_{CO} = 1.25 bar and T = 293 K, and (b) imaged in 'pure' O_2, after the surface had been oxidized in a oxygen-rich CO/O_2 mixture and cooled down to T = 293 K in 'pure' O_2.

In this particular example, working at room temperature would require the use of unrealistically pure gasses. At a gas pressure of 1 bar a trace impurity with a dominant affinity to the surface, present in the gas with a concentration at the 1 ppm level would cover the surface completely within a few milliseconds! Under 'realistic', catalytic conditions, however, the requirements cannot be that extreme. In practical catalysis, a certain tolerance with respect to the cleanliness of the reactants must be acceptable. This implies that if we perform our STM observations during actual reactions, the cleanliness of the gasses is less of an issue. In the present case of CO oxidation, we deliberately mix O_2 and CO gas flows and can definitely tolerate a modest contamination of the O_2 gas with CO. At temperatures above ~400 K, CO desorption becomes significant and the platinum surfaces are no longer poisoned by CO.

What we learn from this example is that for meaningful STM observations of catalytically active surfaces it is best not to merely increase the pressure to the "other side" of the pressure gap but to also operate in a temperature regime where the reaction of interest is running. In practice, this will often require the combination of high pressures and elevated temperatures.

4. Conclusions

In this article, we have reviewed experiments on the oxidation of CO over Pt(110) and Pd(100) model catalyst surfaces, performed with a special-purpose 'Reactor-STM' at atmospheric pressures and elevated temperatures. The configuration of this scanning tunneling microscope, which is integrated with a miniature flow-reactor cell, has allowed us to image the active forms of these surfaces during actual reactions and in combination with fully synchronized, online monitoring of the reaction kinetics.

For both surfaces, we have observed that under O_2 rich conditions surface oxide films form during CO oxidation at atmospheric pressures. In contrast with the traditional view that such oxides would not be active and could actually poison the CO oxidation reaction, we have found them to have superior catalytic activity. Whereas the reaction kinetics on the metallic surfaces reflect the Langmuir–Hinshelwood mechanism, with the reaction taking place between CO molecules and O atoms adsorbed at neighboring sites, the oxides are active via the Mars-Van Krevelen mechanism, in which CO molecules withdraw O atoms directly from the oxide. As a 'side product' of this reaction mechanism, the oxide surfaces become increasingly rough.

We have observed spontaneous oscillations in the CO oxidation rate on Pd(100), which we have identified to be transitions between the metallic surface with its low reactivity and the highly reactive surface oxide.

The stabilization of high-energy surface structures under the influence of the presence of reactants (and products) at high pressures may be viewed as a general consequence of basic thermodynamics and it should therefore be expected to occur also in a variety of other catalytic systems. This underlines the necessity to investigate by experiment and theory the structure of active catalyst surfaces under the conditions of interest, i.e. *during actual catalysis*.

Acknowledgements

This work is supported by the Dutch Technology Foundation (STW), the Foundation for Fundamental Research on Matter (FOM), the Dutch Organization for Scientific Research (NWO). The European Union is acknowledged for financial support under contract no. NMP3-CT-2003-505670 (NANO2).

References

[1] J. Wintterlin, Adv. Catal 45 (2000) 131.
[2] J.A. Rodriguez and D.W. Goodman, Surf. Sci. Rep. 14 (1991) 1.
[3] P. Stoltze and J.K. Nørskov, Phys. Rev. Lett. 55 (1985) 2502.
[4] H. Leideheiser Jr., and A.T. Gwathmey, J. Am. Chem. Soc. 70 (1948) 1200.
[5] R.W. McCabe, T. Pignet and L.D. Schmidt, J. Catal. 32 (1974) 114.
[6] M. Flytzani-Stephanopoulos, S. Wong and L.D. Schmidt, J. Catal. 49 (1977) 51.
[7] A.K. Galwey, P. Gray, J.F. Griffiths and S.M. Hasko, Nature 313 (1985) 668.
[8] M. Baerns, R. Imbihl, V.A. Kondratenko, R. Kraehnert, W.K. Offermans, R.A. van Santen and A. Scheibe, J. Catal. 232 (2005) 226.
[9] X.-G. Wang, W. Weiss, Sh. K. Shaikhutdinov, M. Ritter, M. Petersen, F. Wagner, R. Schlögl and M. SchefflerPhys., Rev. Lett. 81 (1998) 1038.
[10] X.-G. Wang, A. Chaka and M. Scheffler, Phys. Rev. Lett. 84 (2000) 3650.
[11] K. Reuter and M. Scheffler, Phys. Rev. B 65 (2001) 035406.
[12] H. Over, Y.D. Kim, A.P. Seitsonen, S. Wendt, E. Lundgren, M. Schmid, P. Varga, A. Morgante and G. Ertl, Science 287 (2001) 1474.
[13] B.L.M. Hendriksen and J.W.M. Frenken, Phys. Rev. Lett. 89 (2002) 046101.
[14] E. Lundgren, G. Kresse, C. Klein, M. Borg, J.N. Andersen, M. De Santis, Y. Gauthier, C. Konvicka, M. Schmid and P. Varga, Phys. Rev. Lett. 88 (2002) 246103.
[15] B.L.M. Hendriksen, S.C. Bobaru and J.W.M. Frenken, Surf. Sci. 552 (2004) 229.
[16] J. Rogal, K. Reuter and M. Scheffler, Phys. Rev. B 69 (2004) 075421.
[17] E. Lundgren, J. Gustafson, A. Mikkelsen, J.N. Andersen, A. Stierle, H. Dosch, M. Todorova, J. Rogal, K. Reuter and M. Scheffler, Phys. Rev. Lett. 92 (2004) 046101.
[18] A. Stierle, N. Kasper, H. Dosch, E. Lundgren, J. Gustafson, A. Mikkelsen and J.N. Andersen, J. Chem. Phys. 122 (2005) 044706.
[19] J. Gustafson, A. Mikkelsen, M. Borg, E. Lundgren, L. Köhler, G. Kresse, M. Schmid, P. Varga, J. Yuhara, X. Torrelles, C. Quirós and J.N. Andersen, Phys. Rev. Lett. 92 (2004) 126102.
[20] J. Gustafson, A. Mikkelsen, M. Borg, J.N. Andersen, E. Lundgren, C. Klein, W. Hofer, M. Schmid, P. Varga, L. Köhler, G. Kresse, N. Kasper, A. Stierle and H. Dosch, Phys. Rev. B 71 (2005) 115442.
[21] H. Schweiger, P. Raybaud, G. Kresse and H. Toulhoat, J. Catal. 207 (2002) 76.
[22] M. Ackermann, O. Robach, C. Walker, C. Quiros, H. Isern and S. Ferrer, Surf. Sci. 557 (2004) 21.
[23] K. Reuter and M. Scheffler, Phys. Rev. B. (2003) 045407.
[24] G. Ertl, Adv. Catal. 37 (1990) 213.
[25] J. Falta, R. Imbihl and M. Henzler, Phys. Rev. Lett. 64 (1990) 1409.
[26] M. Sander and R. Imbihl, Surf. Sci. 255 (1991) 61.
[27] J.E. Turner, B.C. Sakes and M.B. Maple, Surf. Sci. 103 (1981) 54.
[28] J.E. Turner, B.C. Sales and M.B. Maple, Surf. Sci. 109 (1981) 591.
[29] N. Hartmann, R. Imbihl and W. Vogel, Catal. Lett. 28 (1994) 373.
[30] F.G. Requejo, E.L.D. Hebenstreit, D.F. Ogletree and M. Salmeron, J. Catal. 226 (2004) 83.
[31] W.P.A. Jansen, A.W. Denier v.d. Gon, G.M. Wijers, Y.G.M. Rikers, H.H. Brongersma, J.A.M. de Hoogen P.W.v.d. Laat, T.M. Maas, E.C.A. Dekkers and P. Brinkgreve, Rev. Sci. Instrum. 73 (2002) 354.
[32] P.L. Hansen, J.B. Wagner, S. Helveg, J.R. Rostrup-Nielsen, B.S. Clausen and H. Topsøe, Science 295 (2002) 2053.
[33] G.A. Beitel, A. Laskov, H. Oosterbeek and E.W. Kuipers, J. Phys. Chem. 100 (1996) 12494.
[34] E. Ozensoy, C. Hess, D. Loffreda, P. Sautet and D.W. Goodman, J. Phys. Chem B 109 (2005) 5415.
[35] X. Su, P.S. Cremer, Y.R. Shen and G.A. Somorjai, Phys. Rev. Lett. 77 (1996) 3858.
[36] G. Rupprechter, T. Dellwig, H. Unterhalt and H.-J. Freund, J. Phys. Chem B 105 (2001) 3797.
[37] H.H. Rotermund, Surf. Sci. 386 (1997) 10.
[38] A. Knop-Gericke, M. Hävecker, T. Schedel-Niedrig and R. Schlögl, Catal. Lett. 66 (2000) 215.
[39] H. Isern, K. Peters, P. Steadman, O. Robach, J. Alvarez, E. Lundgren and S. Ferrer, Surf. Sci. 101 (2001) 482–485.
[40] B.J. McIntyre, M. Salmeron, G.A. Somorjai, Rev. Sci. Instrum. 64 (1993).
[41] J.A. Jensen, K.B. Rider, Y. Chen and M. Salmeron, J. Vac. Sci. Technol. B 17 (1999) 1080.
[42] E. Lægsgaard, L. Österlund, P. Thostrup, P.B. Rasmussen, I. Stensgaard and F. Besenbacher, Rev. Sci. Instrum. 72 (2001) 3537.
[43] A. Kolmakov and D.W. Goodman, Rev. Sci. Instrum. 74 (2003) 2444.
[44] M. Rößler, P. Geng and J. Wintterlin, Rev. Sci. Instrum. 76 (2005) 023705.
[45] J.A. Jensen, K.B. Rider, M. Salmeron and G.A. Somorjai, Phys. Rev. Lett. 80 (1998) 1228.
[46] E. Kruse Vestergaard, P. Thostrup, T. An, E. Lægsgaard, I. Stensgaard, B. Hammer and F. Besenbacher, Phys. Rev. Lett 88 (2002) 259601.
[47] P. Cernota, K. Rider, H.A. Yoon, M. Salmeron and G. Somorjai, Surf. Sci. 445 (2000) 249.
[48] K. Rider, K.S. Hwang, M. Salmeron and G.A. Somorjai, Phys. Rev. Lett. 86 (2001) 4330.
[49] K.B. Rider, K.S. Hwang, M. Salmeron and G.A. Somorjai, J. Am. Chem. Soc. 124 (2002) 5588.

[50] P. Thostrup, E. Kruse Vestergaard, T. An, E. Lægsgaard and F. Besenbacher, J. Chem. Phys. 118 (2003) 3724.
[51] B.J. McIntyre, M. Salmeron and G.A. Somorjai, J. Vac. Sci. Technol. A 11 (1993) 1964.
[52] L. Österlund, P.B. Rasmussen, P. Thostrup, E. Lægsgaard, I. Stensgaard and F. Besenbacher, Phys. Rev. Lett. 86 (2001) 460.
[53] A. Kolmakov and D.W. Goodman, Surf. Sci. 490 (2001) L597.
[54] P.B. Rasmussen, B.L.M. Hendriksen, H. Zeijlemaker, H.G. Ficke and J.W.M. Frenken, Rev. Sci. Instrum. 69 (1998) 3879.
[55] B.L.M. Hendriksen, PhD thesis, (Leiden University, 2003).
[56] G. Ertl, Science 254 (1991) 1750.
[57] Selected movies can be viewed via www.phyiscs.leidenuniv.nl/sections/cm/ip.
[58] P. Mars and D.W. Van Krevelen, Spec. Suppl. Chem. Eng. Sci. 3 (1954) 41.
[59] E.P.J. Mallens, J.H.B.J. Hoebink and G.B. Marin, Catal. Lett. 33 (1995) 291.
[60] C. Doornkamp and V. Ponec, J. Molec. Catal. A. Chem. 162 (2000) 19.
[61] K. Itaya, S. Sugawara, K. Sashikata and N. Furuya, J. Vac. Sci. Technol. A 8 (1990) 515.
[62] M. Salmeron, L. Brewer and G.A. Somorjai, Surf. Sci. 112 (1981) 207.
[63] S. Helveg, H.T. Lorensen, S. Horch, E. Lægsgaard, I. Stensgaard, K.W. Jacobsen, J.K. Nørskov and F. Besenbacher, Surf. Sci. 430 (1999) L533.
[64] W.X. Li, L. Österlund, E.K. Vestergaard, R.T. Vang, J. Matthiesen, T.M. Pedersen, E. Lægsgaard, B. Hammer F. Besenbacher, Phys. Rev. Lett. 93 (2004) 146104.
[65] X.-Q. Gong, Z.-P. Liu, R. Raval and P. Hu, J. Am. Chem. Soc. 126 (2004) 8.
[66] X.-Q. Gong, R. Raval and P. Hu, Phys. Rev. Lett. 93 (2004) 106104.
[67] M.D. Ackermann *et al.*, to be published.
[68] S.C. Bobaru *et al.*, to be published.
[69] M.D. Ackermann *et al.*, to be published.
[70] G. Veser, A. Wright and R. Caretta, Catal. Lett. 58 (1999) 199.
[71] M. Saidy, O.L. Warren, P.A. Thiel and K.A.R. Mitchell, Surf. Sci. 494 (2001) L799.
[72] G. Zheng and E.I. Altman, Surf. Sci. 504 (2002) 253.
[73] M. Todorova, E. Lundgren, V. Blum, A. Mikkelsen, S. Gray, J. Gustafson, M. Borg, J. Rogal, K. Reuter, J.N. Andersen and M. Scheffler, Surf. Sci. 541 (2003) 101.
[74] B.L.M. Hendriksen, S.C. Bobaru and J.W.M. Frenken, Catal. Today, 105 (2005) 234.
[75] M.R. Bassett and R. Imbihl, J. Chem. Phys. 93 (1990) 811.
[76] B.C. Sales, J.E. Turner and M.B. Maple, Surf. Sci. 114 (1982) 381.
[77] G. Ertl, M. Neumann and K.M. Streit, Surf. Sci. 64 (1977) 393.
[78] D.C. Tang, K.S. Hwang, M. Salmeron and G.A. Somorjai, J. Phys. Chem. B 108 (2004) 13300.